*inventions*

MDPI

*Article*

# Mathematical Analysis of Two Phase Saturated Nanofluid Influenced by Magnetic Field Gradient

**Farhan Khan * and Xiaodong Yang**

Beijing Key Laboratory of Nonlinear Vibrations and Strength of Mechanical Structures, College of Mechanical Engineering, Beijing University of Technology, Beijing 100124, China; yangxd@bjut.edu.cn
* Correspondence: fkhan@emails.bjut.edu.cn

**Abstract:** Nanofluids are composed of nano-sized particles dispersed in a carrier liquid. The present investigation's aim is to examine theoretically the magneto-thermomechanical coupling phenomena of a heated nanofluid on a stretched surface in the presence of magnetic dipole impact. Fourier's law of heat conduction is used to evaluate the heat transmission rate of the carrier fluids ethylene glycol and water along with suspended nanoparticles of a cobalt–chromium–tungsten–nickel alloy and magnetite ferrite. A set of partial differential equations is transformed into a set of non-linear ordinary differential equations via a similarity approach. The computation is performed in Matlab by employing the shooting technique. The effect of the magneto-thermomechanical interaction on the velocity and temperature boundary layer profiles with the attendant effect on the skin friction and heat transfer is analyzed. The maximum and minimum thermal energy transfer rates are computed for the $H_2O$-$Fe_3O_4$ and $C_2H_6O_2$-$CoCr_{20}W_{15}Ni$ magnetic nanofluids. Finally, the study's results are compared with the previously available data and are found to be in good agreement.

**Keywords:** heat transfer; thermal analysis; ferrite and alloy particle; magnetic dipole; friction drag

check for updates

**Citation:** Khan, F.; Yang, X. Mathematical Analysis of Two Phase Saturated Nanofluid Influenced by Magnetic Field Gradient. *Inventions* **2021**, *6*, 26. https://doi.org/10.3390/inventions6020026

Academic Editor: M. M. Bhatti

Received: 28 February 2021
Accepted: 2 April 2021
Published: 7 April 2021

**Publisher's Note:** MDPI stays neutral with regard to jurisdictional claims in published maps and institutional affiliations.

**Copyright:** © 2021 by the authors. Licensee MDPI, Basel, Switzerland. This article is an open access article distributed under the terms and conditions of the Creative Commons Attribution (CC BY) license (https://creativecommons.org/licenses/by/4.0/).

## 1. Introduction

The problems of fluids' flow and heat transfer for the rate of cooling and heating is very important in various industrial processes, such as polymer extrusion, drawing of plastic and sheets, fiberglass, the production of paper and many more. The transfer of heating or cooling in an object or between two distinct surfaces takes place due to temperature differences. A higher temperature difference causes higher thermal energy transmission [1–3]. The transmission of thermal energy can be computed theoretically using the well known law, i.e., Fourier's law. This law uses the correlation between thermal conductivity and heat capacity to evaluate the transmission rate of thermal energy. The law also states that the transmission of thermal energy occurs with an inertial rate [4–6]. Later on, Cattaneo-Christov [7] added the thermal relaxation time into Fourier's law. It plays an important role when experiments are difficult to conduct for heat transfer simulation. These laws are used for the theoretical computation of heat transfer [8–10]. The above discussed laws are used for evaluation of heat flux in two phase fluids as well as regular fluids.

The boundary layer flows on the stretching sheet has been examined by many researchers for the rate of heat transfer and cooling as it has promising applications in many industries. The stretching sheet velocity of the flow field has gained considerable attention as it has a certain effect on the excellence of the final products in the fabric and polymer industry. This stretching velocity can be linear, polynomial, hyperbolic or exponential. The pioneering work of Crane [11] has laid the foundation for theoretical investigations on the flow field over a stretching surface. He presented an exact analytical solution of the flow over a linearly stretching sheet. The boundary layer heat transport flow of multiphase magnetic fluids past a stretching sheet under the impact of a circular magnetic field was described in [12]. The general fluid model for the magnetohydrodynamic fluid flow and heat transfer was analyzed by Hatzikonstantinou and Vafeas [13]. The authors computed

heat transfer along with the skin friction coefficient in the flow of a micropolar fluid. In this direction, Papadopoulos et al. [14] demonstrated the theoretical investigation of pipe flow in the presence of a magnetic field in a ferrofluid along with a cylindrical coil. The available literature in this direction includes the study of ferrite nanoparticles [15–19].

The literature consists of study of ferrite and regular particles, which are studied in different base fluids for heat transfer along with skin friction. These particles have been studied multiple times with different effects to compute which mathematical model better suits the physical situation. Thus, in the field of fluid dynamics the same problem is normally studied with different effects and parameters to predict the heat transfer that better suits the physical situation modeled. The fluid flow computed for heat transfer and skin friction is available in [20–23].

Ferromagnetic fluids were first synthesized by Rosensweig [24] in his pioneering work, in which he also first used the term ferrohydrodynamics. After that, the work has received increasing attention over the last few decades. In his later detailed work [25], he explored the basic equations for ferromagnetic fluids with internal rotation. The heat transfer is efficient in solids instead of liquids or gasses. Therefore, smart liquids called ferrofluids are synthesized by introducing ferromagnetic nanoparticles into a carrier fluid. The suspension of solid nanoparticles (1–100 nm) in a base fluid enhances the transport properties of the considered nanofluid and hence its heat transfer rate. The ferrofluids are famous due to the suspension of nano-sized ferrite particles instead of regular particles. These ferrite particles have the extra property of Curie temperature; thus, ferrofluids are of great interest and have been studied extensively by researchers after the work of Rosensweig [24]. To make electronic devices long-lasting, ferrofluids can evacuate heat from these devices, such as in speakers and Lenovo laptops [26]. Heat transfer in these devices takes place through the magnetic fluid, made up of a base fluid (water, oil, ethylene glycol) and ferrite nanoparticles. Later on, the flow problem discussed by Crane [11] was extended by Andreson and Valnes [27] with the addition of a magnetic field gradient on the stretched surface of an incompressible non-conducting ferrofluid. Odenbach [28] pointed out the behavior of magnet field impact over magnetite ferrofluid experimentally and discussed the practical applications in technical and medical fields.

In this study, the dynamics of heat transfer processes associated with the motion of viscous , incompressible fluids in the presence of a magnetic field and temperature gradient are analyzed. One of the striking features of the considered nanofluid is the dependence of the magnetization upon the temperature gradient, and this thermomagnetic coupling makes the study of these fluids demanding. Since the suspension of nano-sized particles in a viscous fluid enhances the transport properties of the flowing fluid, the transmission rate of the thermal energy is also enhanced. Therefore, the aim of the article is to describe the interaction between a magnetic field gradient and solid nano-sized particles and its influence on the convection, heat transfer and friction drag.

A cobalt–chromium–tungsten (wolfram)–nickel ($CoCr_{20}W_{15}Ni$) alloy and magnetite ferrite ($Fe_3O_4$) nano-sized particles were added into a base fluid of ethylene glycol ($C_2H_6O_2$) and water ($H_2O$). The graphical results are computed in the discussion section. The particles and the base fluid properties are taken under the assumption of isothermal equilibrium. The analysis is made in such a way that a single solid particle is suspended in the base fluid. The suspension is then computed for thermal energy transmission. The comparison is made for the ferrite ($Fe_3O_4$) and alloy ($CoCr_{20}W_{15}Ni$) two phase nanofluid flow. The results are discussed and presented for the base fluids ethylene glycol ($C_2H_6O_2$) and water ($H_2O$).

## 2. Mathematical Modeling

The steady state two phase incompressible laminar flow in the presence of an external magnetic dipole that is placed near the $x$ surface at distance $l$ is incorporated. The disturbance to the laminar flow is induced via the stretching $x-$surface sheet, and the stretching velocity is defined to be $u = Sx$. The temperature of the fluid at the surface is $T_w$, whereas the temperature of fluid far away from the sheet is taken to be a Curie

temperature, i.e., $T = T_c$. The ferrite $Fe_3O_4$ and alloy $CoCr_{20}W_{15}Ni$ solid nanoparticles satisfy the Curie temperature $T_c$. By contrast, the ferrite $Fe_3O_4$ and alloy $CoCr_{20}W_{15}Ni$ along with the base fluids ethylene glycol $C_2H_6O_2$ and water $H_2O$ are taken under the assumption of isothermal equilibrium and no slip occurs between them.

The vector form of the equation for the flow of the ferrofluid is given in [25]. In vector form the equations for the present problem are:

$$\nabla.\mathbf{V} = 0, \tag{1}$$

$$\rho_{nf}\left(\frac{\partial \mathbf{V}}{\partial t} + \mathbf{V}.\nabla\mathbf{V}\right) = -\nabla P + \mu_{nf}\nabla^2\mathbf{V} + \mu_0 M.\nabla\mathbf{H}, \tag{2}$$

$$(\rho c_p)_{nf}\left(\frac{\partial T}{\partial t} + \mathbf{V}.\nabla T + \mu_0 T\frac{\partial M}{\partial T}\mathbf{V}.\nabla\mathbf{H}\right) = k_{nf}\nabla^2 T, \tag{3}$$

Physically, Equation (1) represents the conservation of mass. The left-hand side of Equation (2) represents momentum due to convection or inertial forces; the first term in Equation (2) on the right-hand side represents the pressure, whereas the second term appears due to surface forces or viscous forces, and the third term denotes the body forces due to the magnetic dipole moment. The first term on the left-hand side of Equation (3) represents heat transfer due to convection, and the second term represents the internal energy due to magnetic dipole. The right-hand side of Equation (3) shows the heat transfer due to conduction.

The mathematical equation for the steady state two-dimensional flow of an incompressible ferrofluid and boundary layer flow described by the dynamical equations governing convective flow and the heat transfer of the nanofluid can be written as:

$$\frac{\partial u}{\partial x} + \frac{\partial v}{\partial y} = 0, \tag{4}$$

$$\rho_{nf}\left(u\frac{\partial u}{\partial x} + v\frac{\partial u}{\partial y}\right) = -\frac{\partial P}{\partial x} + \mu_{nf}\frac{\partial^2 u}{\partial y^2} + \mu_0 M\frac{\partial H}{\partial x}, \tag{5}$$

$$(\rho c_p)_{nf}\left(u\frac{\partial T}{\partial x} + v\frac{\partial T}{\partial y}\right) + (\rho c_p)_{nf}\mu_0 T\frac{\partial M}{\partial T}\left(u\frac{\partial H}{\partial x} + v\frac{\partial H}{\partial y}\right) = k_{nf}\frac{\partial^2 T}{\partial y^2}. \tag{6}$$

The thermo-mechanical coupling at the wall and far from the wall is defined as:

$$u|_{y=0} = Sx, \quad v|_{y=0} = 0, \quad T|_{y=0} = T_w, \tag{7}$$

$$u|_{y\to\infty} \to 0, \quad T|_{y\to\infty} \to T_c. \tag{8}$$

The term $\mu_0 M\frac{\partial H}{\partial x}$ in Equation (5) represents the component of magnetic force per unit volume. This term depends on the existence of the magnetic field gradient along the corresponding x direction, called the Kelvin force, and is very well known in ferrohydrodynamics. The term $\mu_0 T\frac{\partial M}{\partial T}\left(u\frac{\partial H}{\partial x} + v\frac{\partial H}{\partial y}\right)$ in Equation (6) is due to the magneto caloric effect and represents the thermal power per unit of volume.

The relation of the ferrofluid between some of the physical characteristics of the solid nanoparticle and the considered carrier fluid were explained by Islam et al. [29] and is given in Table 1:

**Table 1.** Mathematical expressions of thermo-physical properties.

| Properties | Islam et al. [29] |
|---|---|
| Thermal Conductivity $k$ | $\frac{k_{nf}}{k_f} = \frac{2k_f+k_s-2\Phi(k_f-k_s)}{2k_f+k_s+\Phi(k_f-k_s)}$ |
| Viscosity $\mu$ | $\mu_{nf} = \mu_f(1-\Phi)^{-25/10}$ |
| Heat Capacity $\rho C_p$ | $(\rho c_p)_{nf} = (1-\Phi)(\rho c_p)_f + \Phi(\rho c_p)_s$ |
| Density $\rho$ | $\rho_{nf} = (1-\Phi)\rho_f + \Phi\rho_s$ |

The thermo-physical properties for $C_2H_6O_2$-$Fe_3O_4$, $C_2H_6O_2$-$CoCr_{20}W_{15}Ni$, $H_2O$-$Fe_3O_4$, and $H_2O$-$CoCr_{20}W_{15}Ni$ are given in Table 2.

**Table 2.** Thermo-physical values of $C_2H_6O_2$, $H_2O$, $CoCr_{20}W_{15}Ni$, and $Fe_3O_4$.

| | $k$ (W/mK) | $\rho$ (kg/m$^3$) | $C_p$ (J/kgK) |
|---|---|---|---|
| $CoCr_{20}W_{15}Ni$ | 15 | 9.60 | 400.0 |
| $Fe_3O_4$ | 9.7 | 5180 | 670 |
| $C_2H_6O_2$ | 0.249 | 1116.6 | 2382 |
| $H_2O$ | 0.60 | 998.3 | 4182 |

### *2.1. Magnetic Dipole*

Artificially synthesized nanofluids behave like normal fluids except that they experience a force due to magnetization. One of the striking features of nanofluids is the dependence of magnetization upon the temperature gradient, and this thermomagnetic coupling makes these fluids demanding in various applications. An external magnetic dipole is placed in the flowing fluid to magnetize the two phase $C_2H_6O_2$-$Fe_3O_4$, $C_2H_6O_2$-$CoCr_{20}W_{15}Ni$, $H_2O$-$Fe_3O_4$, and $H_2O$-$CoCr_{20}W_{15}Ni$ nanofluids. The introduction of magnetic forces into the magnetizable liquid gives rise to the effect known as ferrohydrodynamics. Now, since the nanoparticles are mechanically free to align with the fields of lines, the expression of the body force could be a good approximation for the flows of nanofluids. The magnetic scalar potential $\Omega$ is stated below:

$$\Omega = \frac{\gamma_1}{2\pi}\frac{x}{(y+l)^2+x^2}, \tag{9}$$

here $\gamma_1$ symbolizes the dipole moment per unit length, while the $x$ and $y$ components for the magnetic field are:

$$H_x = -\frac{\partial\Omega}{\partial x} = -\frac{\gamma_1}{2\pi}\frac{-(y+d)^2+x^2}{\left(x^2+(y+d)^2\right)^2}, \tag{10}$$

$$H_y = -\frac{\partial\Omega}{\partial y} = \frac{\gamma_1}{2\pi}\frac{2x(y+d)}{\left((y+d)^2+x^2\right)^2}. \tag{11}$$

Since it is generally known that the magnetic body force is relative to the magnetic field gradient of $H$, we have:

$$H = \sqrt{\left(\frac{\partial\Omega}{\partial y}\right)^2 + \left(\frac{\partial\Omega}{\partial x}\right)^2}. \tag{12}$$

Using Equations (10)–(12), and then differentiating the resultant equation with respect to $x$ and $y$, we obtain the following equations:

$$\frac{\partial H}{\partial x} = -\frac{\gamma_1}{\pi}\frac{x}{(y+d)^4}, \tag{13}$$

$$\frac{\partial H}{\partial y} = \frac{\gamma_1}{\pi}\left(\frac{2x^2}{(y+d)^5} - \frac{1}{(y+d)^3}\right). \tag{14}$$

The variation of the magnetization $M$ with the magnetic field intensity $H$ and temperature $T$ can be fairly approximated by the linear relation shown below. The detailed explanation for the derivation of $H$ is presented in [27]. The magnetization is defined as:

$$M = K_c(T - T_\infty). \tag{15}$$

The geometry for the two phase $C_2H_6O_2$-$Fe_3O_4$, $C_2H_6O_2$-$CoCr_{20}W_{15}Ni$, $H_2O$-$Fe_3O_4$, and $H_2O$-$CoCr_{20}W_{15}Ni$ nanofluids is evident in Figure 1.

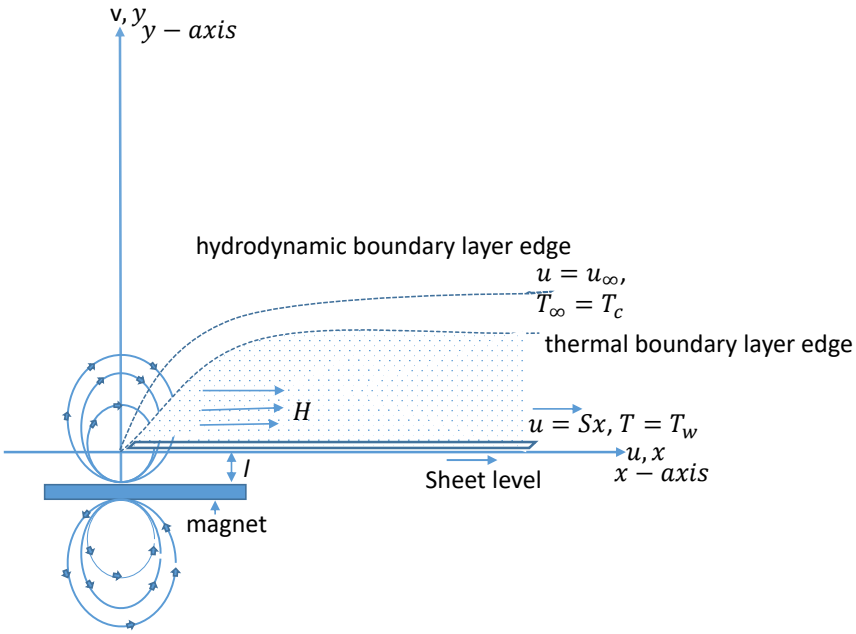



**Figure 1.** Geometrical representation of the flow.

### 2.2. Similarity Analysis

For the numerical solution of the governing boundary layer model, Equations (5) and (6), along with boundary conditions, need to be transformed into non-dimensional ordinary differential equations. The transformations is performed by introducing the similarity analysis. The similarity transformation for the two phase nanofluid introduced by Andersson and Valnes [27] is:

$$\begin{aligned} \psi(\xi,\eta) &= \left(\frac{\mu_f}{\rho_f}\right)\eta f(\xi), \\ \theta(\eta,\xi) &\equiv \frac{T - T_c}{T_w - Tc} = \theta_1(\xi) + \eta^2\theta_2(\xi). \end{aligned} \tag{16}$$

The stream function $\psi(x,y)$ defined by the velocity components is $u = \frac{\partial \psi}{\partial y}, v = -\frac{\partial \psi}{\partial x}$, which satisfies the conservation Equation (4) identically, while $f$ and $\theta$ are the dimensionless functions.

$$\begin{aligned} \xi &= y\left(\frac{\rho_f S}{\mu_f}\right)^{\frac{1}{2}}, & u &= Sxf'(\xi), \\ \eta &= x\left(\frac{\rho_f S}{\mu_f}\right)^{\frac{1}{2}}, & v &= -\left(S\nu_f\right)^{\frac{1}{2}} f(\xi). \end{aligned} \tag{17}$$

By using Equations (16) and (17) in the momentum and energy Equations (5) and (6), we obtain the transformed nonlinear ordinary differential equations of the momentum and temperature as follows:

$$\frac{A_1^{-1}}{(1-\Phi)^{\frac{25}{10}}} f''' + ff'' - (f')^2 - \frac{2A_1^{-1}\beta\theta_1}{(\xi+\gamma)^4} = 0, \tag{18}$$

$$\frac{A_2^{-1}k_{nf}}{k_f}\theta_1'' + Pr(f\theta_1' - 2f'\theta_1) - 4A_2^{-1}\sigma_2(f')^2 + \frac{2A_2^{-1}\sigma_2\beta f(\theta_1-\sigma_1)}{(\xi+\gamma)^3} = 0, \tag{19}$$

$$\begin{aligned} &\frac{A_2^{-1}k_{nf}}{k_f}\theta_2'' - Pr(4f'\theta_2 - f\theta_2') + \frac{2A_2^{-1}\sigma_2\beta f\theta_2}{(\xi+\gamma)^3} \\ &- \frac{\beta(\theta_1-\sigma_1)}{(\xi+\gamma)^3}\left(\frac{4f}{(\xi+\gamma)^5} + \frac{2f'}{(\xi+\gamma)^4}\right) - A_2^{-1}\sigma_2(f'')^2 = 0, \end{aligned} \tag{20}$$

The boundary conditions in (6) and (7) now become:

$$\begin{aligned} &f'(\xi) = 1, \quad f(\xi) = 0, \quad \theta_1(\xi) = 1, \quad \theta_2(\xi) = 0, \quad at \quad \xi = 0, \\ &f'(\xi) \to 0, \quad \theta_1(\xi) \to 0, \quad \theta_2(\xi) \to 0, \quad at \quad \xi \to \infty, \end{aligned} \tag{21}$$

while $A_1$ and $A_2$ are:

$$A_1 = 1 - \Phi + \Phi\frac{\rho_s}{\rho_f}, \qquad A_2 = 1 - \Phi + \Phi\frac{\rho c_{ps}}{\rho c_{pf}}. \tag{22}$$

The dimensionless parameters calculated in the problem include $\beta$ (ferrohydrodynamic interaction), $\sigma_2$ (viscous dissipation), $Pr$ (Prandtl number), and $\sigma_1$ (dimensionless Curie temperature). Mathematical expressions are presented below:

$$\begin{aligned} \sigma_1 &= \frac{T_c}{T_w - T_c}, \qquad \beta = \frac{\gamma_1}{2\pi}\frac{\mu_0 K_c(T_w - T_c)\rho_f}{\mu_f^2}, \\ \sigma_2 &= \frac{S\mu_f^2}{\rho_f K_c(T_w - T_c)}, \quad \gamma = \sqrt{\frac{S\rho_f l^2}{\mu_f}}, \qquad Pr = \frac{\nu_f}{\alpha_f}. \end{aligned} \tag{23}$$

The physical interest parameters for the boundary layer flow problems are the skin friction coefficient, which is the rate of shear stress, and the Nusselt number, which is the rate of heat transfer. The wall shear stress characterized by the skin friction coefficient $C_f$, along with the Nusselt number, is:

$$\begin{aligned} C_f &= \frac{\tau_w}{\frac{1}{2}\rho_{nf}S^2}, \qquad \tau_w = \mu_{nf}\left.\frac{\partial u}{\partial y}\right|_{y=0}, \\ Nu_x &= \frac{xk_{nf}}{k_f(T_w - T_c)}\left.\frac{\partial T}{\partial y}\right|_{y=0}. \end{aligned} \tag{24}$$

where $q_w = -k_{nf}\left(\frac{\partial T}{\partial y}\right)_{y=0}$ is the surface heat flux. The substitution of the non-dimensional similarity transformation considered in Equations (16) and (17) into Equation (24) transforms the skin friction and local Nusselt number into dimensionless form. Hence, Equation (24) takes the following form:

$$\begin{aligned} \frac{1}{2}Re_x^{\frac{1}{2}}C_f &= \frac{1}{(1-\Phi)^{\frac{25}{10}}}f''(0), \\ Re_x^{-\frac{1}{2}}Nu_x &= \frac{-k_{nf}}{k_f}\Big(\theta_1'(0) + \eta^2\theta_2'(0)\Big). \end{aligned} \tag{25}$$

where the local Reynolds number $Re_x$ is defined as $Re_x = xS/\nu_f$, which is based on the stretching sheet velocity $S_{(x)}$.

## 3. Numerical Simulation

The non-linear ordinary differential momentum (Equations (18)) and energy equations (Equations (19) and (20)), together with the appropriate boundary conditions (Equation (21)) were solved numerically using the shooting technique for various values of physical parameters. The mathematical model for the ferromagnetic two phase $C_2H_6O_2$-$Fe_3O_4$, $C_2H_6O_2$-$CoCr_{20}W_{15}Ni$, $H_2O$-$Fe_3O_4$, and $H_2O$-$CoCr_{20}W_{15}Ni$ nanofluids was computed with the help of the shooting technique in Matlab. The analysis in the discussion section is based on the dimensionless parameters and numbers in the above equations. The results show the impact of the solid particles on the heat transfer rate and friction drag theoretically. The system of equations is transformed into the first order equations in order to solve via the shooting technique.

$$\begin{aligned} &W_1 = f(\xi), W_2 = f'(\xi), W_3 = f''(\xi), W_3' = f'''(\xi), W_4 = \theta_1(\xi), \\ &W_5 = \theta_1'(\xi), W_5' = \theta_1''(\xi), W_6 = \theta_2(\xi), W_7 = \theta_2'(\xi), W_7' = \theta_2''(\xi). \end{aligned} \tag{26}$$

Using the transformation given in Equation (26), it reduces the Equations (18)–(21):

$$\begin{aligned} W_3' &= (1-\Phi)^{\frac{25}{10}}A_1\left(W_2 * W_2 - W_3 * W_1 + \frac{2\beta W_4}{A_1(\xi+\gamma)^4}\right), \\ W_5' &= -\frac{k_f A_2}{k_{nf}}\left(Pr(W_5W_1 - 2W_4W_2) + \frac{2\lambda\beta W_4(W_1-\varepsilon)}{A_2(\xi+\gamma)^3} - \frac{4\lambda}{A_2}W_2^2\right), \\ W_7' &= \frac{k_f A_2}{k_{nf}}\left(Pr(4W_6W_2 - W_7W_1) - \frac{2\lambda\beta W_1W_6}{A_2(\xi+\gamma)^3} + \frac{\lambda}{A_2}W_2^2\right. \\ &\quad \left. + \frac{\lambda\beta(W_4-\varepsilon)}{(\xi+\gamma)^3}\left(\frac{2W_2}{(\xi+\gamma)^4} + \frac{4W_1}{(\xi+\gamma)^5}\right)\right), \end{aligned} \tag{27}$$

$$\begin{aligned} &W_1 = 1, W_2 = 0, W_4 = 1, W_6 = 0, \quad at \quad \xi = 0, \\ &W_2 \to 0, W_4 \to 0, W_6 \to 0, \quad at \quad \xi \to \infty. \end{aligned} \tag{28}$$

## 4. Discussion

The two phase $C_2H_6O_2$-$Fe_3O_4$, $C_2H_6O_2$-$CoCr_{20}W_{15}Ni$, $H_2O$-$Fe_3O_4$, and $H_2O$-$CoCr_{20}W_{15}Ni$ magnetic nanofluids were computed via the shooting technique in Matlab. The influence of physical parameters and dimensionless numbers on the flowing magnetic nanofluid is discussed in this section. Two base fluids along with two distinct solid particles are examined. The ferrite and alloy nanoparticles are entertained in the analysis. The magnetic two phase $C_2H_6O_2$-$Fe_3O_4$, $C_2H_6O_2$-$CoCr_{20}W_{15}Ni$, $H_2O$-$Fe_3O_4$, and $H_2O$-$CoCr_{20}W_{15}Ni$ nanofluids are simulated. The flows of $C_2H_6O_2$-$Fe_3O_4$, $C_2H_6O_2$-$CoCr_{20}W_{15}Ni$, $H_2O$-$Fe_3O_4$, and $H_2O$-$CoCr_{20}W_{15}Ni$ nanofluids were computed and then compared with each other. The variation of velocity field was noticed to be in an order, $H_2O$-$Fe_3O_4$, $H_2O$-$CoCr_{20}W_{15}Ni$,

$C_2H_6O_2$-$Fe_3O_4$, and $C_2H_6O_2$-$CoCr_{20}W_{15}Ni$. Therefore, we conclude that the maximum velocity field is determined for the $H_2O$-$Fe_3O_4$ nanofluid and the minimum distribution of velocity is determined for the magnetic $C_2H_6O_2$-$CoCr_{20}W_{15}Ni$ nanofluid. This variation occurs due to the thermophysical values of the transport properties of the solid particles and base fluids. The comparison is shown in Figure 2. The relation is compared for the temperature field in Figure 3. The variation in temperature distribution is noticed in the order $C_2H_6O_2$-$CoCr_{20}W_{15}Ni$, $C_2H_6O_2$-$Fe_3O_4$, $H_2O$-$CoCr_{20}W_{15}Ni$, and $H_2O$-$Fe_3O_4$. This means that the $H_2O$-$Fe_3O_4$ nanofluid leads to the lowest temperature, whereas the $C_2H_6O_2$-$CoCr_{20}W_{15}Ni$ magnetic nanofluid exhibits the higher temperature field. The ferrite nanoparticles considered in the problem have higher thermal properties, which help in the enhancement of heat transfer; as a result, the lower temperature field occurs for the magnetite ferrite base magnetic nanofluid. Cobalt particles, however, have the property of Curie temperature, but that is not sufficient for a higher temperature field. Thus, the lower temperature field is observed for the alloy-based magnetic nanofluid.

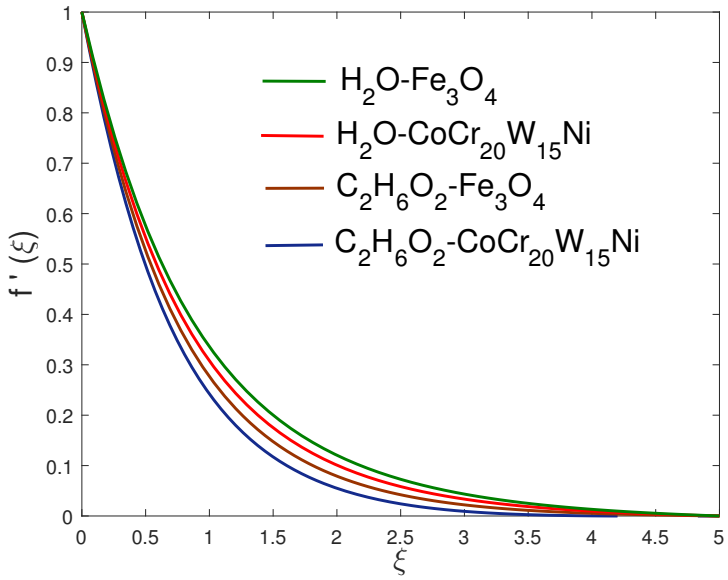



**Figure 2.** Velocity field comparison of magnetic nanofluids $C_2H_6O_2$-$Fe_3O_4$, $C_2H_6O_2$-$CoCr_{20}W_{15}Ni$, $H_2O$-$Fe_3O_4$, and $H_2O$-$CoCr_{20}W_{15}Ni$.

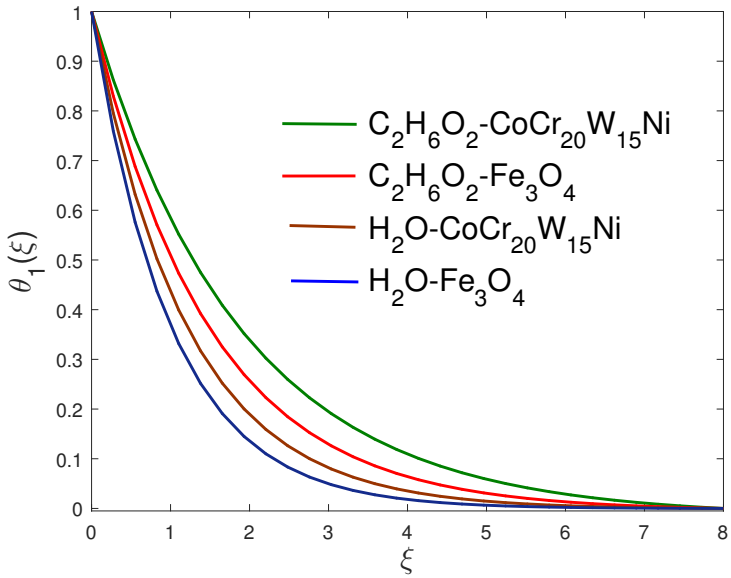



**Figure 3.** Temperature field comparison of magnetic nanofluids $C_2H_6O_2$-$Fe_3O_4$, $C_2H_6O_2$-$CoCr_{20}W_{15}Ni$, $H_2O$-$Fe_3O_4$, and $H_2O$-$CoCr_{20}W_{15}Ni$.

The influence of ferrohydrodynamic interaction parameter $\beta$ on the temperature and the axial velocity is displayed in Figures 4 and 5. The magnetic property of the solid particles, i.e., alloys and ferrite, makes the two phase nanofluid magnetize in the presence of a magnetic dipole placed near the surface. The dipole attracts the alloy and the ferrite particles until the alloy and ferrite reach their Curie temperature. Thus, the axial velocity for varying $\beta$ declines, whereas the temperature profile for $\beta$ shows the reverse nature for all of the magnetic nanofluids $C_2H_6O_2$-$Fe_3O_4$, $C_2H_6O_2$-$CoCr_{20}W_{15}Ni$, $H_2O$-$Fe_3O_4$, and $H_2O$-$CoCr_{20}W_{15}Ni$. The impact of $\beta$ on the axial velocity is determined in Figure 4, whereas its influence on the temperature field is evident in Figure 5. The interaction between the nanoparticles of the ferrite and alloys with the flowing fluid leads to resisting the flow and the internal energy of the fluid. The higher resistance to the flowing fluid is induced by the alloy as well as the ferrite nanoparticles; as a result, the velocity field declines, as presented in Figure 4. On the other hand, the internal energy in the presence of the alloy and ferrite nanoparticles arises when $\beta$ is enhanced; thus, the temperature field enhancement is evident, as shown in Figure 5.

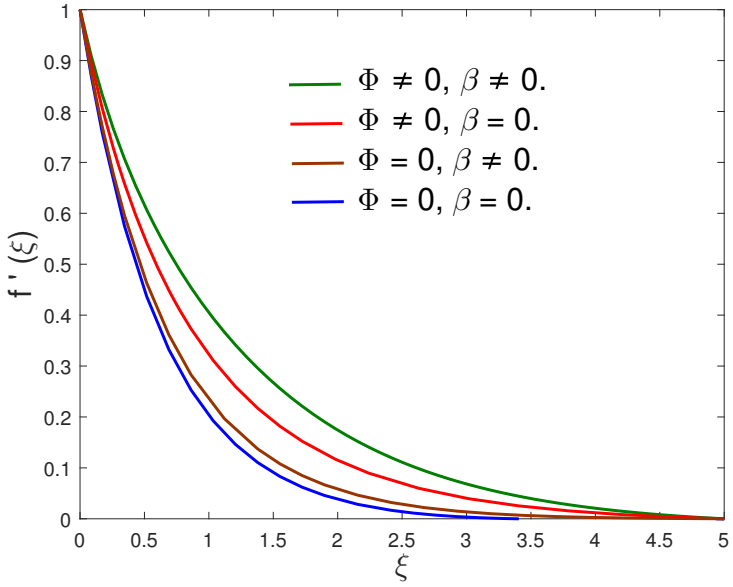



**Figure 4.** Influence of $\beta$ on the velocity of magnetic nanofluids $C_2H_6O_2$-$Fe_3O_4$, $C_2H_6O_2$-$CoCr_{20}W_{15}Ni$, $H_2O$-$Fe_3O_4$, and $H_2O$-$CoCr_{20}W_{15}Ni$.

Generally, thermal engineers are interested in the reduction of wall shear stresses, whilst they need to enhance the heat transfer rate of the system. For this purpose, the mathematician constructs different mathematical models that interpret the heat transfer and the fluid flow to examine which model better predicts the friction drag and Nusselt number. Regular fluids have low thermal properties; thus, they are not fast in transmission of thermal energy, whereas solids have higher transport properties, and hence their dispersion in base fluids make them more efficient for heat transfer. Therefore, $C_2H_6O_2$-$Fe_3O_4$, $C_2H_6O_2$-$CoCr_{20}W_{15}Ni$, $H_2O$-$Fe_3O_4$, and $H_2O$-$CoCr_{20}W_{15}Ni$ magnetic nanofluids were incorporated in this work. A higher resistance induced by the surface to the flowing fluid was noticed for the $C_2H_6O_2$-$CoCr_{20}W_{15}Ni$ magnetic fluid, which indicates that the alloy particles can cause more resistance as compared to the ferrite nanoparticles, as evident in Figure 6. The higher resistance has a better impact on the corresponding velocity. This means that the corresponding velocity will be higher for the considered solid particle and the base fluid. Figure 7 demonstrates the Nusselt number for the $C_2H_6O_2$-$Fe_3O_4$, $C_2H_6O_2$-$CoCr_{20}W_{15}Ni$, $H_2O$-$Fe_3O_4$, and $H_2O$-$CoCr_{20}W_{15}Ni$ magnetic nanofluids. The maximum transmission of heat is observed for the $H_2O$-$Fe_3O_4$ magnetic nanofluid. The thermal properties are higher for the base fluid as well as for the solid ferrite nanoparticles. Thus, the maximum heat transfer is noticed for the $H_2O$-$Fe_3O_4$ magnetic nanofluid, while

the temperature behavior is lowered. A comparison of the present results was made with the available results examined by Ishak et al. [30]. The comparison is made for the Nusselt number as presented in Table 3.

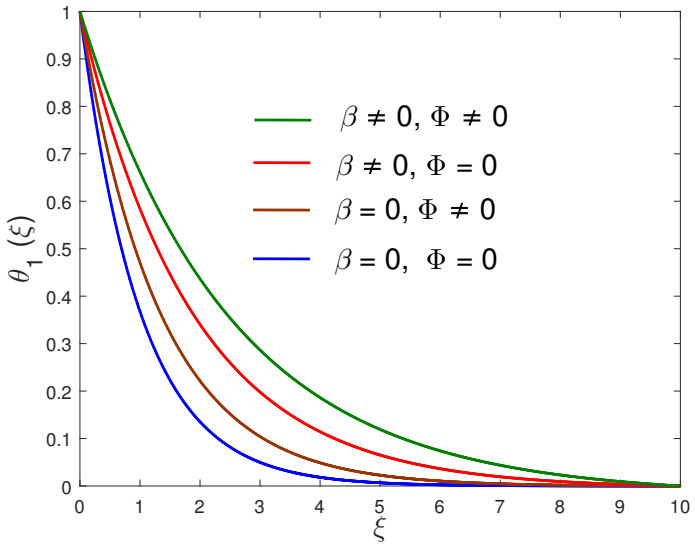



**Figure 5.** Influence of $\beta$ on the temperature of magnetic nanofluids $C_2H_6O_2$-$Fe_3O_4$, $C_2H_6O_2$-$CoCr_{20}W_{15}Ni$, $H_2O$-$Fe_3O_4$, and $H_2O$-$CoCr_{20}W_{15}Ni$.

**Table 3.** Comparison of Nusselt number for various values of Pr (Prandtl number) in the flow of $C_2H_6O_2$, $H_2O$, $CoCr_{20}W_{15}Ni$, and $Fe_3O_4$.

| Pr | Ishak et al. [30] | Present Results |
|---|---|---|
| 0.01 | 0.0197 | 0.0155 |
| 0.72 | 0.8086 | 0.8088 |
| 1.0 | 1.0000 | 1.0000 |
| 3.0 | 1.9237 | 1.9298 |
| 7.0 | 3.0723 | 3.0765 |
| 10.0 | 3.7207 | 3.7200 |
| 100.0 | 5.2941 | 5.2965 |

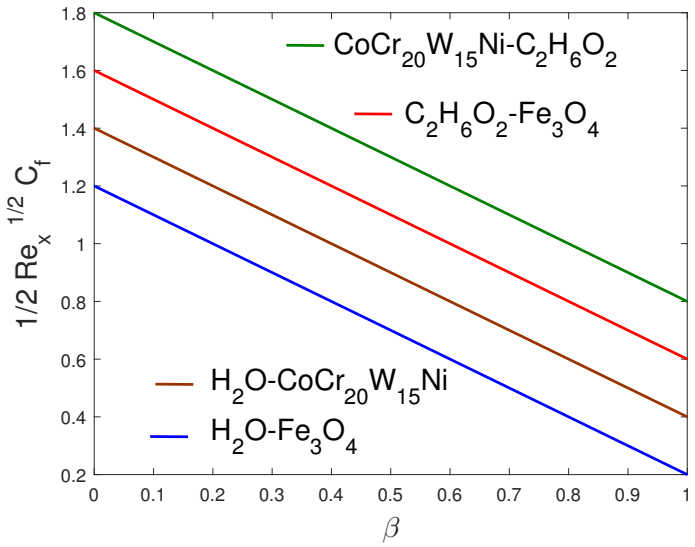



**Figure 6.** Comparison of wall shear stress in the flow of magnetic nanofluids $C_2H_6O_2$-$Fe_3O_4$, $C_2H_6O_2$-$CoCr_{20}W_{15}Ni$, $H_2O$-$Fe_3O_4$, and $H_2O$-$CoCr_{20}W_{15}Ni$.

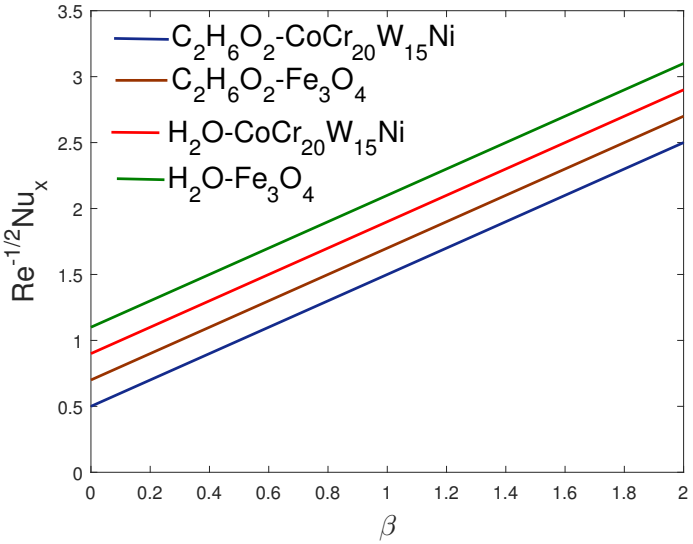



**Figure 7.** Comparison of Nusselt number in magnetic nanofluids $C_2H_6O_2$-$Fe_3O_4$, $C_2H_6O_2$-$CoCr_{20}W_{15}Ni$, $H_2O$-$Fe_3O_4$, and $H_2O$-$CoCr_{20}W_{15}Ni$.

## 5. Concluding Remarks

The phenomena of heat transfer analysis in ferromagnetic nanofluids on a stretching surface was explored with nanoparticles of magnetite ferrite and alloy in water and ethylene glycol (EG) as a carrier fluid. The main objective of the present theoretical study was to reduce the friction drag in the boundary layer flow and to intensify the efficiency of the considered nanofluid. The characteristics of nanoparticles together with the magnetic dipole impact enhanced the thermal conductivity of the engineered nanofluid and hence their influence on the heat flow. An appropriate transformation was employed on the mathematical model to convert the described system of partial differential equations into nonlinear ordinary differential equations and then computations were performed using the shooting method.

Combinations of nanoparticles of ferrite magnetite with a base fluid of water and ethylene glycol, and then of a cobalt–chromium–tungsten–nickel alloy in water and EG were examined. Moreover, the impact of various physical parameters involved in the flow model, such as ferrohydrodynamics interaction and others, were also analyzed on the velocity and temperature profiles to predict heat transfer rate. Finally, a comparison of different values of the Prandtl number indicated excellent agreement with previous data available in the literature. In conclusion, the nanofluid $H_2O$-$Fe_3O_4$ was found to exhibit a maximum heat transfer rate and $C_2H_6O_2$-$CoCr_{20}W_{15}Ni$ with higher resistance as compared to the rest of the nanofluid combinations considered.

**Author Contributions:** F.K. and X.Y. have read and agreed to the published version of the manuscript. All authors have read and agreed to the published version of the manuscript.

**Funding:** This research received no external funding.

**Institutional Review Board Statement:** Not applicable.

**Informed Consent Statement:** Not applicable.

**Data Availability Statement:** Not applicable.

**Conflicts of Interest:** The authors declare no conflict of interest.

## Nomenclature

| | |
|---|---|
| $u, v$ | Velocity components |
| $(\rho c_p)_{nf}$ | Specific heat of hybrid nanofluid |
| $\mu_{nf}$ | Dynamic viscosity |
| $k_{nf}$ | Thermal conductivity ofhybrid nanofluid |
| $\rho_{nf}$ | Density of hybrid nanofluid |
| $T$ | Temperature |
| $P$ | Pressure |
| $M$ | Magnetization |
| $S$ | Stretching rate |
| $T_c$ | Curie temperature |
| $Re_x$ | Reynolds number |
| $K_c$ | Pyromagnetic coefficient |
| $C_f$ | Skin friction |
| $\rho_{nf}$ | density of hybrid nanofluid |
| $Nu_x$ | Nusselt number |
| $\gamma_1$ | Magnetic field induction |
| $H$ | Magnetic field |
| $\Omega$ | Magnetic scalar potential function |

## References


1. Ross, R.G.; Andersson, P.; Sundqvist, B.; Backstrom, G. Thermal conductivity of solids and liquids under pressure. *Rep. Prog. Phys.* **1984**, *47*, 1347. [CrossRef]
2. Zeller, R.C.; Pohl, R.O. Thermal conductivity and specific heat of noncrystalline solids. *Phys. Rev. B* **1971**, *4*, 2029. [CrossRef]
3. Zhang, S.; Zhou, H.; Wang, H. Thermal conductive properties of solid-liquid-gas three-phase unsaturated concrete. *Constr. Build. Mater.* **2020**, *232*, 117242. [CrossRef]
4. Attri, R.; Roychowdhury, S.; Biswas, K.; Rao, C.N.R. Low thermal conductivity of 2D borocarbonitride nanosheets. *J. Solid State Chem.* **2020**, *282*, 121105. [CrossRef]
5. Malheiros, F.C.; Gomes do Nascimento, J.; Fernandes, A.P.; Guimares, G. Simultaneously estimating the thermal conductivity and thermal diffusivity of a poorly conducting solid material using single surface measurements. *Rev. Sci. Instrum.* **2020**, *91*, 014902. [CrossRef] [PubMed]
6. Ahmed, S.E.; Mansour, M.A.; Alwatban, A.M.; Aly, A.M. Finite element simulation for MHD ferro-convective flow in an inclined double-lid driven L-shaped enclosure with heated corners. *Alex. Eng. J.* **2020**, *59*, 217–226. [CrossRef]
7. Christov, C.I. On frame indifferent formulation of the Maxwell-Cattaneo model of finite speed heat conduction. *Mech. Res. Commun.* **2009**, *36*, 481–486. [CrossRef]
8. Yan, L.; Zhang, M.; Wang, M.; Guo, Y.; Zhang, X.; Xi, J.; Yuan, Y.; Mirzasadeghi, A. Bioresorbable mg-based metastable nano-alloys for orthopedic fixation devices. *J. Nanosci. Nanotechnol.* **2020**, *20*, 1504–1510. [CrossRef]
9. Chen, J.; Liu, L.; Deng, J. Spin Orbit Torque-Based Spintronic Devices Using L10-Ordered Alloys, National University of Singapore (SG). U.S. Patent No. 10,741,749, 2020.
10. Liu, X.; Sammarco, C.; Zeng, G.; Guo, D.; Tang, W.; Tan, C.K. Investigations of monoclinic-and orthorhombic-based $(B_xGa_{1-x})_2O_3$ alloys. *Appl. Phys. Lett.* **2020**, *117*, 012104. [CrossRef]
11. Crane, L.J. Flow past a stretching plate. *Z. FüR Angew. Math. Und Phys. Zamp.* **1970**, *21*, 645–647. [CrossRef]
12. Zeeshan, A.; Majeed, A.; Fetecau, C.; Muhammad, S. Effects on heat transfer of multiphase magnetic fluid due to circular magnetic field over a stretching surface with heat source/sink and thermal radiation. *Results Phys.* **2017**, *7*, 3353–3360. [CrossRef]
13. Hatzikonstantinou, P.M.; Vafeas, P. A general theoretical model for the magnetohydrodynamic flow of micropolar magnetic fluids. Application to Stokes flow. *Math. Methods Appl. Sci.* **2010**, *33*, 233–248. [CrossRef]
14. Papadopoulos, P.K.; Vafeas, P.; Hatzikonstantinou, P.M. Ferrofluid pipe flow under the influence of the magnetic field of a cylindrical coil. *Phys. Fluids* **2012**, *24*, 122002. [CrossRef]
15. Siddique, A.R.M.; Venkateshwar, K.; Mahmud, S.; Van Heyst, B. Performance analysis of bismuth-antimony-telluride-selenium alloy-based trapezoidal-shaped thermoelectric pallet for a cooling application. *Energy Convers. Manag.* **2020**, *222*, 113245. [CrossRef]
16. Ramesh, G.K.; Shehzad, S.A.; Rauf, A.; Chamkha, A.J. Heat transport analysis of aluminum alloy and magnetite graphene oxide through permeable cylinder with heat source/sink. *Phys. Scr.* **2020**, *95*, 095203. [CrossRef]
17. Gupta, M.; Singh, V.; Said, Z. Heat transfer analysis using zinc Ferrite/water (Hybrid) nanofluids in a circular tube: An experimental investigation and development of new correlations for thermophysical and heat transfer properties. *Sustain. Energy Technol. Assess.* **2020**, *39*, 100720. [CrossRef]

18. Ajith, K.; Enoch, I.M.; Solomon, A.B.; Pillai, A.S. Characterization of magnesium ferrite nanofluids for heat transfer applications. *Mater. Today Proc.* **2020**, *27*, 107–110. [CrossRef]
19. Kirithiga, R.; Hemalatha, J. Investigation of thermophysical properties of aqueous magnesium ferrite nanofluids. *J. Mol. Liq.* **2020**, *2*, 113944. [CrossRef]
20. Gupta, M.; Das, A.; Mohapatra, S.; Das, D.; Datta, A. Surfactant based synthesis and magnetic studies of cobalt ferrite. *Appl. Phys. A* **2020**, *126*, 1–13. [CrossRef]
21. Izadi, A.; Siavashi, M.; Rasam, H.; Xiong, Q. MHD enhanced nanofluid mediated heat transfer in porous metal for CPU cooling. *Appl. Therm. Eng.* **2020**, *168*, 114843. [CrossRef]
22. Jyothi Sankar, P.R.; Venkatachalapathy, S.; Asirvatham, L.G. Thermal performance enhancement studies using graphite nanofluid for heat transfer applications. *Heat Transf.* **2020**, *49*, 3013–3029. [CrossRef]
23. Fourier, B.J. *The Analytical Theory of Heat*; Translated by Alexander Freeman; Cambridge University Press: London, UK, 1878.
24. Rosensweig, R.E. Nestor JW and Timmins RS. *AlChE Symp. Ser.* **1965**, *5*, 104–118.
25. Rosensweig, R.E. Basic equations for magnetic fluids with internal rotations. In *Ferrofluids*; Springer: Berlin/Heidelberg, Germany, 2002; pp. 61–84.
26. Bououdina, M.; Manoharan, C. Dependence of structure/morphology on electrical/magnetic properties of hydrothermally synthesised cobalt ferrite nanoparticles. *J. Magn. Magn. Mater.* **2020**, *493*, 165703.
27. Andersson, H.I.; Valnes O.A. Flow of a heated ferrofluid over a stretching sheet in the presence of a magnetic dipole. *Acta Mech.* **1998**, *2*, 39–47. [CrossRef]
28. Odenbach, S. Magnetic fluids-suspensions of magnetic dipoles and their magnetic control. *J. Phys. Condens. Matter* **2003**, *15*, S1497. [CrossRef]
29. Islam, S.; Zubair, M.; Tassaddiq, A.; Shah, Z.; Alrabaiah, H.; Kumam, P.; Khan, W. Unsteady Ferrofluid Slip Flow in the Presence of Magnetic Dipole with Convective Boundary Conditions. *IEEE Access* **2020**, *8*, 138551–138562. [CrossRef]
30. Ishak, A.; Nazar, R.; Pop, I. Boundary layer flow and heat transfer over an unsteady stretching vertical surface. *Meccanica* **2009**, *44*, 369–375. [CrossRef]